The *Hoja loca1* Mutant and AUX/IAA Function in Maize

Richardson A. E.[1,2,#], Sluis A.[1,2,#], Hake S.*[1,2],

(1)USDA Plant Gene Expression Center, 800 Buchanan Street, Albany, CA 94710.

(2)Department of Plant and Microbial Biology, University of California Berkeley, CA.

*corresponding author

[#]these authors contributed equally to the article.

Author Contributions:

SH conceived the original project, developed the mapping population and secured funding. AR and AS designed and carried out the experiments. AR and SH wrote the manuscript. SH agrees to serve as the author responsible for contact and ensures communication.

One Line Summary:

The maize AUX/IAA ZmIAA38 is involved in phytomer coordination, aerial organ initiation and mediolateral patterning, and illustrates species specific sub-functionalization of the AUX/IAAs.

Abstract

Auxin plays a vital role in plant organ development, influencing organ initiation and patterning across all axes. The diversity in auxin patterning results from changes in the activities and expression of auxin signaling components, including the AUX/IAA repressors. Higher land plants have multigene AUX/IAA families, which leads to functional redundancy and a lack of phenotype in loss of function mutants. Instead, dominant mutations, which prevent AUX/IAA degradation in response to auxin, have highlighted the importance of these proteins in organ development. Here we report a new dominant AUX/IAA mutant in maize, *Hoja loca1* (*Oja*). *Oja* has a mutation in the degron motif of ZmIAA28 and affects aerial organ initiation and medio-lateral patterning in the leaf. These phenotypes contrast with other maize AUX/IAA mutants that affect the root or inflorescence only. *Oja* illustrates the role of auxin signaling in the tight coordination of phytomer unit development and provides evidence of species-specific sub-functionalization of the AUX/IAAs.

Introduction

The iterative post-embryonic development of plants has led to impressive developmental plasticity, which allows plants to modify their architecture over time and respond to environmental conditions. Organs initiate from meristems, groups of self-organizing totipotent cells, in regular phyllotactic patterns. Initiation of each leaf includes an axillary meristem and an internode. This developmental unit of leaf, axillary meristem, and internode is known as a phytomer. Aerial plant development can therefore be understood as the successive formation of phytomer units (Galinat, 1959), with developmental plasticity manifesting in different amounts of growth in the three components.

The fate of cells within the meristem is dependent on position. Cells in the center of shoot meristems divide slowly, are isodiametric in shape, and are considered indeterminate. As divisions push cells from the center outward, cells enter the peripheral or morphogenetic zone, where organs initiate. It is here that the primordium is specified, forming a leaf at plastochron 0 (P_0) (Bolduc et al., 2012a). The *KNOTTED1-LIKE HOMEOBOX* (*KNOX*) genes mark indeterminate cell fates (Jackson et al., 1994; Smith et al., 1992), and are down-regulated in P_0 cells. *KNOX* gene expression is maintained within the other components of the phytomer, the internode and bud, until they elongate (Tsuda et al., 2017). The downregulation of *KNOX* genes in the P_0 is preceded by the formation of an auxin maximum, coordinated by a convergence point of the auxin transporter PINFORMED1 (PIN1) in the epidermis (Bayer et al., 2009; Benkova et al., 2003; O'Connor et al., 2014; Reinhardt et al., 2003). Auxin acts by triggering the degradation of AUX/IAA proteins, allowing AUXIN RESPONSE FACTORS (ARFs) to regulate downstream genes (Lavy and Estelle, 2016; Salehin et al., 2015). These coordinated events comprise the mechanism for organ initiation.

As organs develop and differentiate, asymmetries are established that determine tissue identity across proximal/distal, abaxial/adaxial, and medial/lateral axes (Kuhlemeier and Timmermans, 2016; Richardson and Hake, 2019). In grasses, the leaf initiates as a ring-shaped primordium around the meristem with the separation of the lower leaf (sheath) margins occurring later in development (Johnston et al., 2015; Sharman, 1942). Proximal-

distal patterning in the grass leaf leads to the formation of a distal blade and a proximal sheath. The ligule and auricle form at the boundary of blade and sheath. For most grasses, the medial/lateral axes are marked by a midvein at the center which is thickened in comparison with the margins of the leaf (referred to as the midrib).

Auxin signaling has been implicated in all stages and axes of grass leaf development. Treatment of maize shoot apices, with the auxin inhibitor NPA (*N-1*-Naphthylphthalamic Acid) limits organ initiation and prevents the separation of the sheath margins resulting in a tube leaf (Scanlon, 2003). PIN proteins are also expressed at the position of a ligule prior to its elaboration (Moon et al., 2013) and RNAseq analysis of leaf microdomains has shown that ligule development involves the recapitulation of the organ initiation mechanism (Johnston et al., 2014). The establishment of the abaxial/adaxial axis also involves auxin signaling, utilizing opposing gradients of tasiR-ARFs and miR166 (Nogueira et al., 2007). Despite the role of auxin signaling throughout grass leaf development, auxin signaling mutants (i.e. mutants in AUX/IAA or ARFs) which affect leaf development have not yet been reported in grasses.

Here we describe a dominant mutant, named *Hoja loca1* (*Oja*), with a range of leaf defects. In its most severe expression, mutants fail to initiate leaves although an internode will be partitioned to each phytomer. In the least severe, midveins are missing from otherwise correctly patterned leaves. In between these extremes, tube leaves are formed where the leaf margin is completely fused. Remarkably, leaves maintain proximal distal and abaxial/adaxial patterning. Using positional cloning and whole genome sequencing, we identify the gene as the Aux/IAA protein, *ZmIAA28* (GRMZM2G035465). Unlike other maize Aux/IAA mutants that specifically affect roots (Woll et al., 2005) or inflorescences (Galli et al., 2015), *Oja* provides a view into the unique role of Aux/IAA proteins in grass leaf patterning. The ability of *Oja* to produce a leafless phytomer also hints at the role of auxin signaling in coordinating development of the separate phytomer components.

Results

Isolation of *Hoja loca1*

94 *Hoja loca1* (*Oja*) was discovered by a forward genetic approach. Pollen of the Mo17 maize
95 inbred was treated with ethyl methanesulfonate (EMS) and crossed onto the B73 inbred.
96 Hybrid F1 seed were planted in the field and screened. The single mutant plant was open
97 pollinated and crossed to multiple inbreds the following season. Further crosses
98 established the dominance of the mutant phenotype although often less than 50% of the
99 plants showed the phenotype, indicating low phenotypic penetrance.
100 Each generation displayed unpredictable variability in phenotypic expression ranging
101 from mild to severe. Crosses made with mildly affected plants gave rise to severe plants
102 and vice versa. Due to the severity of the phenotype, homozygotes were rarely obtained,
103 thus the observations are exclusively with heterozygotes. Analysis was carried out in
104 plants with at least four backcrosses to B73.
105

106 ***Hoja loca1* leaves have medial/lateral defects but normal proximal/distal and**
107 **abaxial/adaxial patterning**

108 Maize leaves are divided into a proximal sheath that wraps around the inner leaves and
109 a distal blade that bends away from the plant, optimized for photosynthesis (Figure 1Ai,iv).
110 At the junction of the blade and sheath is the ligule, an epidermal fringe on the adaxial
111 surface and two auricles along the margin that allow the blade to tilt away from the sheath
112 (Figure 1Aii-iv). The blade contains a midrib, a thickened region with chlorophyll-
113 containing cells on the abaxial surface and clear cells on the adaxial surface (Figure 1Av).
114 The midrib provides stiffness to the extended blade.
115 In contrast to wild-type seedlings, *Hoja loca1* (*Oja*) mutants have varied leaf
116 phenotypes (Figure 1B,C). Mutant and normal-appearing leaves may be present on the
117 same plant. The mildest phenotype includes missing midribs as shown for leaf 2 in Figure
118 1Bi. These leaves drooped backwards without the structural support of the midrib (Figure
119 1Bi-v). The midribless leaves completely lacked adaxial clear cells, although the flanking
120 blade regions appeared normal (Figure 1Bv). Midribless leaves still had normal ligules
121 and auricles (Figure 1Bii-iv) suggesting that the midrib is not essential in elaboration of
122 proximal/distal patterning.
123 The severe phenotype includes tube leaves in which the margins are not separated
124 (Figure 1C). As in the case for midribless leaves, tube leaves also have normal

125 proximal/distal patterning, developing a normal ligule between the sheath and blade
126 (Figure Cii-iv). Cells in the tube leaves also have correct abaxial/adaxial polarity with
127 chlorophyll containing cells on the abaxial surface and clear cells on the adaxial surface
128 (Figure 1Cv). These results suggest that *Oja* does not influence proximal/distal or
129 abaxial/adaxial patterning.

130 To determine whether there was a pattern in initiation of tube or midribless leaves,
131 we recorded the occurrence of midribless and tube leaves in a population of 150 plants
132 (Figure 1D). Both midribless and tube leaves can be observed in the same plant. In all
133 cases, the first leaf is never affected. The second leaf may show one of these defects and
134 the third and fourth are most likely to be mutant (Figure 1D). The frequency for both
135 defects decreases during development but tube leaves could be observed late in
136 development.

137 In many *Oja* plants inflorescence branching and floral development was severely
138 affected. Both male and female inflorescences bore bare regions indicative of a failure to
139 initiate spikelet primordia, and the tassels were not branched. However, when flowers did
140 form, they appeared to be normal and fertile (Supplementary Figure 1). In contrast to
141 aerial development, root development in seedlings appeared to be normal with initiation
142 of primary, seminal and lateral roots and a normal gravitropic response (Figure 2).

143

144 ***Hoja loca1* leaves have defects in vein distribution, but normal vein density.**

145 Given the midrib defect, we next questioned whether veins were altered in *Oja* mutants.
146 Seedling leaf cross-sections showed that the abaxial/adaxial patterning of vascular
147 bundles appeared normal (Figure 3A,B), mirroring the normal abaxial/adaxial patterning
148 of the entire organ.

149 To assess whether the medio-lateral patterning of vascular bundles was altered.
150 we measured leaf width and determined vein density and distribution in the third leaf of
151 3-week-old seedlings. Midribless leaves were narrower than wild type and tube leaves
152 were less than half the width of wild type (Figure 3C). Overall vein density was not affected
153 by *Oja* (Figure 3D) suggesting a reduction in total vein number to match the decrease in
154 size. To assess vein distribution, we counted the number of intermediate veins between
155 lateral veins in both wild-type and midribless leaves. In wild type, the number of

156 intermediate veins shows a symmetry across the leaf, with a dip at the mid position
157 (Figure 3Eii, blue). We did not identify a dip of intermediate veins in the midvein position
158 in *Oja* midribless leaves (Figure 3Eii, orange), supporting the hypothesis that medio-
159 lateral patterning is affected in the *Oja* mutant.
160
161 ***Hoja loca1* mutants fail to initiate leaves but still set aside internode cells**
162 At each leaf initiation, cells are set aside for the leaf and the internode below (Johri and
163 Coe, 1983). A mature maize plant is thus composed of alternating internodes and nodes,
164 which is the position of leaf insertion. In mature *Oja* plants we observed bare nodes, for
165 example the plant in Figure 4A ended in a tube leaf after four nodes failed to elaborate
166 leaves (arrows in the close-up). To assess whether these bare nodes were due to ectopic
167 nodes, or to lack of leaf initiation, we took advantage of maize morphology. In mature
168 maize plants the nodes are morphologically distinct, forming a raised ring around the
169 stem. We counted the number of nodes in *Oja* versus wild-type siblings and compared
170 these to the number of leaves. In mature plants there is no significant difference in total
171 node number (Figure 4B), but there are significantly fewer leaves in *Oja* mutants (Figure
172 4C). This alternating node, internode, node pattern without accompanying leaves is also
173 observed when slicing through developing tubes leaves (Figure 4D). These data suggest
174 that *Oja* may be able to initiate new phytomers consisting of just nodes and internodes.
175 To identify whether leaves failed to initiate, or whether they initiated but failed to
176 elaborate, we used scanning electron microscopy (SEM) to look at the earliest primordial
177 stages of leaf development. Wild-type maize leaves at the P_1 stage are a ring of cells that
178 surround the meristem. At P_2, the leaf begins to grow in the proximal distal dimension,
179 with growth highest at the midvein position. By P_3, the leaf primordium covers the top of
180 the meristem and the margins begin to expand (Figure 4E). Further growth of the leaf
181 margins at the P_4 stage envelopes the younger leaves and meristem (Hay and Hake,
182 2004; Scanlon et al., 1996). Longitudinal growth of the internode and sheath occur later
183 in development.
184 Compared to wild-type seedlings where developing leaf primordia always
185 obscured the internodes, the internodes were often visible in severe *Oja* shoots (Figure
186 4F-I). The meristem in Figure 4F had a single ring primordium which may have been the

early stages of a tube leaf, below this no older leaves were initiated leaving an elongated, exposed internode. The meristem in Figure 4G initiated five internodes without leaves, before more leaf primordia were initiated. In some *Oja* mutants, the leaf initiation defect was so severe that the shoot apex ended in pin-like barren meristems as in Figure 3H. In many mutants, axillary meristems formed which contained more normal leaf initiation (Figure 4I). In fact, the mature plant in Figure 4A had a fertile tiller although the main shoot ended in a tube leaf with skipped leaf initiation. The SEM data suggest that the discrepancy between node number and leaf number in *Oja* is due to patterning during the earliest stages of leaf primordium initiation. This finding supports the hypothesis that *Oja* mutants fail to initiate leaves, despite initiating new phytomers.

The skipped leaf initiation also explains some of the seedling architecture differences. For example, the normal seeding in Figure 1A has four visible leaves while the seeding in Figure 1B has only three leaves visible and the second leaf is the size of a normal third leaf. In addition, the distance between the first and second leaf is much greater than in the wild type. This observation suggests that leaf two was skipped in the mutant.

Meristem markers are not patterned correctly in *Hoja loca1* mutants.

To determine whether the patterning underlying primordium initiation is affected in the *Oja* mutant, we looked at markers of P_0 specification. Given the variability in the *Oja* phenotype within and between plants, we focused on *in situ* markers of patterning, rather than whole plant expression changes.

We first used antibodies to KNOTTED1 (KN1) (Smith et al., 1992) in order to follow leaf initiation defects in the meristem. KN1 accumulates in the meristem and unexpanded stem and is down-regulated at the P_0 region, remaining off in normal maize leaves (Figure 5A). In *Oja* mutants, we see strong accumulation at the tip of the meristem but unlike the normal meristem, the down-regulation appears on both sides of the meristem, suggesting that this P_0 encircles the meristem (Figure 5B). The encircling downregulation could be indicative of a tube leaf initiating. This particular meristem has also failed to initiate at least two leaves and KN1 expression is still maintained in the internode region below the meristem (Figure 5B).

218 Preceding *KNOX* downregulation, the auxin efflux transporter PIN1 moves auxin
219 in the epidermis to the site of leaf initiation. From the P_0, PIN1 proteins move auxin toward
220 pre-existing vasculature, predicting the path of provascular traces (Reinhardt et al., 2003).
221 In many species outside of the *Brassica*, PIN1 proteins have duplicated and diversified
222 function. Sister of PIN1 (SoPIN1) localizes at the leaf initiation site and is also detected
223 in vasculature in grasses (O'Connor et al., 2014). To determine whether SoPIN1
224 patterning was defective in *Oja* meristems, we used an antibody to SoPIN1 to detect
225 protein accumulation at the P_0 site and in the developing pre-vascular strand in wild-type
226 plants (Figure 5C). In wild-type meristems, SoPIN1 convergence points form in the
227 epidermis of the meristem at the P_0, which persists through to the tip of the P_1 leaf (Figure
228 5C). In the *Oja* mutant shown, which has a number of skipped leaf initiations and appears
229 as a pin, the SoPIN1 localization is throughout the tip of the meristem rather than
230 localizing strongly to the P_0 region (Figure 5D). Normal accumulation and polarization can
231 be seen in a vein trace within the mutant meristem. This result suggests that SoPIN1 can
232 polarize and be coordinated across the tissue, but it fails to form a strong convergence
233 point needed at the P_0 in *Oja*, implying that IAA28 may be involved in feedback regulation
234 of SoPIN1 at lateral organ initiation sites.
235 The duplicate YABBY transcription factors DROOPING LEAF (DL) (Strable et al.,
236 2017) are early markers of leaf patterning and are expressed at the P_0 and at the midrib
237 in leaf primordia. To explore the effect of *Oja* on *DL* expression, we used *in situ*
238 hybridization. In the normal seedling, expression was detected in the P_0 and each
239 subsequent midvein region (Figure 5E). In the *Oja* mutant shown, *DL* expression was
240 similar at the midvein region in normal developing leaves, however, there was no
241 detectable expression in the P_0 and fewer leaves had initiated. As DL is involved in midrib
242 specification (Strable et al., 2017), this lack of DL in the P_0 could be due to the lack of leaf
243 initiation or due to the formation of a midribless leaf. Nevertheless, as an early marker of
244 leaf patterning this expression pattern supports the hypothesis that *Oja* mutants fail to
245 specify the P_0 leaf correctly despite defining the rest of the phytomer.
246 In summary, meristem and leaf initiation markers are functional in *Oja* mutants, but
247 their positional placement is altered. This finding suggests that *Oja* has a defect in leaf

248 initiation and patterning, not just leaf outgrowth, which leads to the reduced leaf number
249 compared to node number.
250
251 ***Hoja loca1* encodes the Aux/IAA protein, ZmIAA28**.
252 To identify the causal mutation, we mapped the Mo17 *Oja* region in a backcross
253 population to A619. Bulk segregant mapping placed *Oja* on chromosome 8 (Figure 6A).
254 SSR primers were used to narrow the position to an interval of 1 Mb containing 19
255 annotated genes (Figure 6Aiii). Using published RNAseq data we narrowed the candidate
256 gene list further, as only 10 genes in the interval were reported as expressed in the shoot
257 apical meristem or leaf primordia (Figure 6Aiii, green).
258 To further map the interval, we used whole genome sequencing of two bulk pools,
259 one wild type and one mutant pool each with 40 individuals. A large interval was detected
260 between 75 and 135 Mb. To generate a candidate SNP list, we removed SNPs reported
261 in the HapMapv3 from Panzea (www.panzea.org/data) and limited the reported SNPs to
262 EMS-type G to A or C to T. Within the large interval, there were nine moderate or high-
263 effect SNPs within annotated gene models (Figure 6Ai), but only one SNP detected within
264 the fine SSR mapping interval (Figure 6Aiii, *). This change was a C to T nucleotide
265 transition in GRMZM2G035465, which encodes Aux/IAA28 (Figure 6B). The C to T
266 transition causes a missense mutation from a Glycine to Glutamic Acid in the center of
267 the highly conserved degron motif (Figure 6C). Similar mutations in other AUX/IAA
268 proteins prevent degradation in response to high auxin (Reed, 2001) suggesting that *Oja*
269 is caused by a stabilizing mutation in the degron motif which prevents degradation of
270 ZmIAA28 in the presence of auxin.
271
272 **DISCUSSION**
273 The dominant *Hoja loca1* (*Oja*) mutant specifically affects aerial organ initiation
274 and medial/lateral patterning in the leaf. Positional cloning identified the gene as the
275 Aux/IAA protein ZmIAA28. Aux/IAA proteins function as repressors in low auxin
276 conditions by interacting with ARF transcription factors and preventing their activation of
277 auxin responsive genes. An increase in auxin promotes an interaction between Aux/IAA
278 and Transport Inhibitor Response1 (TIR1), an F-box component of the SCF complex that

279 targets proteins for degradation. Binding of Aux/IAA to TIR1 in the presence of auxin leads
280 to Aux/IAA degradation and thus releases ARF repression (Dharmasiri et al., 2005;
281 Kepinski and Leyser, 2005). As the Aux/IAA gene family is large, redundancy has mostly
282 hidden loss-of-function phenotypes (Overvoorde et al., 2005). Instead, genetic analysis
283 has identified dominant Aux/IAA mutations that stabilize these normally short-lived
284 proteins by disrupting their proteolysis or reducing their ability to bind to TIR1 (Ouellet et
285 al., 2001; Ramos et al., 2001; Tian et al., 2003; Worley et al., 2000; Yang et al., 2004).
286 Most mutations, including *Oja*, are located in domain II in the highly conserved degron
287 motif (Fukaki et al., 2002; Nagpal et al., 2000; Rogg et al., 2001; Rouse et al., 1998;
288 Zenser et al., 2001) which interacts with TIR1 in the presence of auxin (Tan et al., 2007).
289 Nine clades of AUX/IAA proteins have been identified (Matthes et al., 2019),
290 allowing for significant subfunctionalization during the evolution of the AUX/IAA family.
291 The majority of *Arabidopsis* Aux/IAA mutants were first described by their agravitopric
292 root, reduced lateral roots, and/or shorter root phenotypes (Fukaki et al., 2002; Nagpal et
293 al., 2000; Rouse et al., 1998). Mutants that were identified by a shoot phenotype such as
294 *bodenlos*, *Shy2*-2 and *axr3* have pleiotropic phenotypes, also affecting the roots. For
295 example, the semi-dominant *Shy2* mutant was identified as a suppressor of a
296 phytochrome elongated hypocotyl phenotype but also has root defects and curled leaves
297 (Reed et al., 1998; Tian and Reed, 1999). Embryonic patterning defects were identified
298 in *bodenlos* homozygotes but mature heterozygous plants also have root defects
299 (Hamann et al., 2002). *Axr3* mutants develop curled leaves (Leyser et al., 1996; Pérez-
300 Pérez et al., 2010) due to defects in coordination between the abaxial and adaxial
301 surfaces of the leaf. When these mutant phenotypes are mapped to the AUX/IAA clades,
302 no obvious pattern is observed, suggesting that function is not conserved within a clade.
303 This finding highlights the importance of studying the specific function of AUX/IAA
304 proteins in multiple species, as genetic similarity is unlikely to correspond to related
305 functionality.
306 Aux/IAA mutants in maize appear to be less pleiotropic than *Arabidopsis*; their
307 defects are confined to specific parts of the plant. For example, the *rootless with*
308 *undetectable meristem* (*rum1*) mutant is deficient in primary and lateral root initiation with
309 no defects in the aerial parts (Woll et al., 2005). *rum1* encodes *ZmIAA10* and, unlike other

310 described AUX/IAA mutants that have a missense mutation in the degron, *rum1* carries
311 a deletion that includes the GWPPV degron sequence in domain II (von Behrens et al.,
312 2011). The *Bif1* (ZmIAA27) and *Bif4* (ZmIAA20) Aux/IAA mutants reduce the branching
313 in male and female inflorescences (Barazesh et al., 2009; Galli et al., 2015), however,
314 there is no effect on vegetative growth (Galli et al., 2015). *Oja* mutants have striking
315 defects in leaf development but have normal roots and flowers if they make
316 inflorescences. This suggests that ZmIAA10, ZmIAA20, ZmIAA27 and ZmIAA28 have
317 tissue-specific functions. These specificities do not appear to arise from tissue specific
318 expression as, based on published RNAseq data, ZmIAA27 and ZmIAA28 have similar
319 expression patterns. *RUM1* is expressed at very low levels compared to a close paralog
320 which is expressed at high levels in many root tissues as well as the leaf (Zhang et al.,
321 2015). Perhaps the tissue specificity results from the interaction of each Aux/IAA with
322 different ARFs or different TIR proteins and these are responsible for the observed
323 phenotypes in the dominant mutants (Salehin et al., 2015).

324 The variability of the *Oja* phenotype is not unusual, having also been observed in
325 other AUX/IAA mutants such as in the *Arabidopsis* mutant *bodenlos,* with some mutants
326 missing hypocotyl and root and others just missing a root (Hamann et al., 2002). This
327 phenotypic stochasticity could arise from over- and under-compensation of the auxin
328 signaling network.

329 Through investigating leaf initiation, we found that SoPIN1 failed to converge at
330 the P_0 in *Oja* mutants suggesting that ZmIAA28 plays a role in the feedback signaling
331 required for forming the convergence point that triggers organ initiation. A role for the
332 TIR/ARF/AUX/IAA module in regulating cellular polarisation has also been observed in
333 *Arabidopsis* in which induction of the ARF, *MONOPTEROS* (MP) in the *mp* mutant
334 background triggered spontaneous PIN1 convergence point formation and primordium
335 outgrowth in the normally barren *mp* meristem (Bhatia et al., 2016). Interestingly,
336 although leaf initiation was severely affected in *Oja*, many other organ initiation events
337 occurred normally. For example, ligule development requires reactivation of the organ
338 initiation pathway (Johnston et. al., 2014) but *Oja* mutants have no ligule defect,
339 suggesting that different AUX/IAAs may be involved in ligule development.

340 Given that formation of the SoPIN1 convergence point at the P_0 stimulates midvein
341 development, it is likely that ZmIAA28 is required for the signaling that promotes midrib
342 formation at the midvein, influencing medio-lateral patterning and possibly subsequent
343 *DL* expression. Supporting the role of auxin signaling upstream of *DL* expression,
344 DAPseq analyses in maize have identified ARF binding sites upstream of both maize *DL*
345 genes (Galli et al., 2018). In midribless *Oja* mutant leaves, the midrib domain appears to
346 be completely lost, which is more severe than in the *dl* double mutant (Strable et al.,
347 2017), suggesting that other factors, also influenced by auxin signaling, are required to
348 specify midrib differentiation in addition to DL.
349 Our work suggests that ZmIAA28 acts specifically during aerial organ initiation,
350 potentially upstream of *KNOX* downregulation. This contrasts with the function of the
351 tomato class VIII AUX/IAA, SlIAA9. Tomato leaf margin complexity is dependent on the
352 ectopic expression of *KNOX* genes in the leaf lamina. However, reduction of SlIAA9
353 expression causes a loss of leaf margin complexity, independent of *KNOX* gene
354 expression as determined by RT-PCR (Wang et al., 2005). This suggests that although
355 ZmIAA28 and SlIAA9 are in the same clade, they differ in their relationship with *KNOX*
356 gene regulation.
357 The phytomer consists of a node, internode, axillary bud and organ. To maintain
358 correct plant architecture, the development of each component is tightly regulated. *Oja* is
359 unusual in that this coordination within the phytomer unit is apparently broken, allowing
360 the initiation of nodes and internodes without accompanying organs. This finding
361 suggests that auxin is not only involved in the initiation of organs, but also in the regulation
362 of phytomer development as a whole.
363
364 The *Oja* mutant illustrates the species-specific subfunctionalisation of the AUX/IAA
365 proteins in regulating plant development. In contrast to other known AUX/IAAs, ZmIAA28
366 specifically affects initiation of aerial organs and impacts medio-lateral patterning. As
367 further studies identify functions of other grass AUX/IAAs it will be of interest to compare
368 them to *Oja* to see how far this subfunctionalisation holds. This will be particularly
369 interesting to compare to *Arabidopsis aux/iaa* mutants which appear to be more
370 pleiotropic, and to determine the reasons for the species-specific differences.

Acknowledgements

With thanks to Samuel Leiboff and China Lunde for extensive help and advice. ARS microscopy staff and UC Berkeley greenhouse staff. This work was funded by NSF BIO/BBSRC1547062 and ARS 5335-21000-013-00D.

References

Barazesh, S., Nowbakht, C., McSteen, P., 2009. sparse inflorescence1, barren inflorescence1 and barren stalk1 promote cell elongation in maize inflorescence development. Genetics 182, 403-406.

Bayer, E.M., Smith, R.S., Mandel, T., Nakayama, N., Sauer, M., Prusinkiewicz, P., Kuhlemeier, C., 2009. Integration of transport-based models for phyllotaxis and midvein formation. Genes Dev. 23, 373-384.

Benkova, E., Michniewicz, M., Sauer, M., Teichmann, T., Seifertova, D., Jurgens, G., Friml, J., 2003. Local, efflux-dependent auxin gradients as a common module for plant organ formation. Cell 115, 591-602.

Bhatia, N., Bozorg, B., Larsson, A., Ohno, C., Jönsson, H., Heisler, M.G., 2016. Auxin acts through MONOPTEROS to regulate plant cell polarity and pattern phyllotaxis. Current Biology 26, 3202-3208.

Bolduc, N., O'Connor, D., Moon, J., Lewis, M., Hake, S., 2012a. How to pattern a leaf. Cold Spring Harb Symp Quant Biol. 77, 47-51.

Bolduc, N., Yilmaz, A., Mejia-Guerra, M.K., Morohashi, K., O'Connor, D., Grotewold, E., Hake, S., 2012b. Unraveling the KNOTTED1 regulatory network in maize meristems Genes & Development 26, 1685-1690.

Chen, J., Dellaporta, S., 1994. Urea-based Plant DNA Miniprep, in: Freeling, M., Walbot, V. (Eds.), The Maize Handbook. Springer-Verlag, New York, pp. 526-538.

Coen, E.S., Romero, J., Doyle, S., Elliott, R., Murphy, G., Carpenter, R., 1990. floricaula: a homeotic gene required for flower development in Antirrhinum majus. Cell 63, 1311-1322.

Conti, L., Bradley, D., 2007. TERMINAL FLOWER1 is a mobile signal controlling Arabidopsis architecture. The Plant Cell 19, 767-778.

402 Dharmasiri, N., Dharmasiri, S., Estelle, M., 2005. The F-box protein TIR1 is an auxin
403 receptor. Nature 435, 441-445.
404 Fukaki, H., Tameda, S., Masuda, H., Tasaka, M., 2002. Lateral root formation is blocked by a
405 gain-of-function mutation in the SOLITARY-ROOT/IAA14 gene of Arabidopsis. The Plant
406 Journal 29, 153-168.
407 Galinat, W.C., 1959. The phytomer in relation to the floral homologies in the American
408 Maydea. Bot. Mus. Lefl., Harvard Univ. 19, 1-32.
409 Galli, M., Khakhar, A., Lu, Z., Chen, Z., Sen, S., Joshi, T., Nemhauser, J.L., Schmitz, R.J.,
410 Gallavotti, A., 2018. The DNA binding landscape of the maize AUXIN RESPONSE FACTOR
411 family. Nature communications 9, 4526.
412 Galli, M., Liu, Q., Moss, B.L., Malcomber, S., Li, W., Gaines, C., Federici, S., Roshkovan, J.,
413 Meeley, R., Nemhauser, J.L., 2015. Auxin signaling modules regulate maize inflorescence
414 architecture. Proceedings of the National Academy of Sciences 112, 13372-13377.
415 Hamann, T., Benkova, E., Bäurle, I., Kientz, M., Jürgens, G., 2002. The Arabidopsis
416 BODENLOS gene encodes an auxin response protein inhibiting MONOPTEROS-mediated
417 embryo patterning. Genes & development 16, 1610-1615.
418 Hay, A., Hake, S., 2004. The dominant mutant *Wavy auricle in blade1* disrupts patterning in
419 a lateral domain of the maize leaf. Plant Physiol. 135, 300-308.
420 Jackson, D., Veit, B., Hake, S., 1994. Expression of maize *KNOTTED1* related homeobox genes
421 in the shoot apical meristem predicts patterns of morphogenesis in the vegetative shoot.
422 Development 120, 405-413.
423 Johnston, R., Leiboff, S., Scanlon, M.J., 2015. Ontogeny of the sheathing leaf base in maize
424 (Zea mays). New Phytol. 205, 306-315.
425 Johnston, R., Wang, M., Sun, Q., Sylvester, A.W., Hake, S., Scanlon, M.J., 2014. Transcriptomic
426 Analyses Indicate That Maize Ligule Development Recapitulates Gene Expression Patterns
427 That Occur during Lateral Organ Initiation. Plant Cell 12, 4718-4732.
428 Johri, M.M., Coe, E.H., 1983. Clonal analysis of corn plant development. I. The development
429 of the tassel and the ear shoot. Developmental Biology 97, 154-172.
430 Kepinski, S., Leyser, O., 2005. The Arabidopsis F-box protein TIR1 is an auxin receptor.
431 Nature 435, 446-451.

432 Kuhlemeier, C., Timmermans, M.C., 2016. The Sussex signal: insights into leaf
433 dorsiventrality. Development 143, 3230-3237.
434 Lavy, M., Estelle, M., 2016. Mechanisms of auxin signaling. Development 143, 3226-3229.
435 Leyser, H.O., Pickett, F.B., Dharmasiri, S., Estelle, M., 1996. Mutations in the AXR3 gene of
436 Arabidopsis result in altered auxin response including ectopic expression from the SAUR-
437 AC1 promoter. The Plant Journal 10, 403-413.
438 Matthes, M.S., Best, N.B., Robil, J.M., Malcomber, S., Gallavotti, A., McSteen, P., 2019. Auxin
439 evodevo: conservation and diversification of genes regulating auxin biosynthesis,
440 transport, and signaling. Molecular plant 12, 298-320.
441 Moon, J., Candela, H., Hake, S., 2013. The Liguleless narrow mutation affects proximal-distal
442 signaling and leaf growth. Development 140, 405-412.
443 Nagpal, P., Walker, L.M., Young, J.C., Sonawala, A., Timpte, C., Estelle, M., Reed, J.W., 2000.
444 AXR2 encodes a member of the Aux/IAA protein family. Plant physiology 123, 563-574.
445 Nogueira, F.T., Madi, S., Chitwood, D.H., Juarez, M.T., C., T.M., 2007. Two small regulatory
446 RNAs establish opposing fates of a developmental axis. Genes Dev. 21, 750-755.
447 O'Connor, D.L., Runions, A., Sluis, A., Bragg, J., Vogel, J., Prusinkiewicz, P., Hake, S., 2014. A
448 division in PIN-mediated patterning during lateral organ initiation in grasses. PLoS Comput
449 Biol 10, e1003447.
450 Ouellet, F., Overvoorde, P.J., Theologis, A., 2001. IAA17/AXR3: biochemical insight into an
451 auxin mutant phenotype. The Plant Cell 13, 829-841.
452 Overvoorde, P.J., Okushima, Y., Alonso, J.M., Chan, A., Chang, C., Ecker, J.R., Hughes, B., Liu, A.,
453 Onodera, C., Quach, H., 2005. Functional genomic analysis of the AUXIN/INDOLE-3-ACETIC
454 ACID gene family members in Arabidopsis thaliana. The Plant Cell 17, 3282-3300.
455 Pérez-Pérez, J.M., Candela, H., Robles, P., López-Torrejón, G., Del Pozo, J.C., Micol, J.L., 2010.
456 A role for AUXIN RESISTANT3 in the coordination of leaf growth. Plant and cell physiology
457 51, 1661-1673.
458 Ramos, J.A., Zenser, N., Leyser, O., Callis, J., 2001. Rapid degradation of auxin/indoleacetic
459 acid proteins requires conserved amino acids of domain II and is proteasome dependent.
460 The Plant Cell 13, 2349-2360.
461 Reed, J.W., 2001. Roles and activities of Aux/IAA proteins in Arabidopsis. Trends in plant
462 science 6, 420-425.

463 Reed, J.W., Elumalai, R.P., Chory, J., 1998. Suppressors of an Arabidopsis thaliana phyB
464 mutation identify genes that control light signaling and hypocotyl elongation. Genetics 148,
465 1295-1310.
466 Reinhardt, D., Pesce, E.R., Stieger, P., Mandel , T., Baltensperger, K., Bennett, M., Traas, J.,
467 Friml, J., Kuhlemeier, C., 2003. Regulation of phyllotaxis by polar auxin transport. Nature
468 426, 255-260.
469 Richardson, A., Hake, S., 2019. Drawing a Line: Grasses and Boundaries. Plants 8, 4.
470 Richardson, A., Rebocho, A.B., Coen, E., 2016. Ectopic KNOX expression affects plant
471 development by altering tissue cell polarity and identity. The Plant Cell 28, 2079-2096.
472 Rogg, L.E., Lasswell, J., Bartel, B., 2001. A gain-of-function mutation in IAA28 suppresses
473 lateral root development. The Plant Cell 13, 465-480.
474 Rouse, D., Mackay, P., Stirnberg, P., Estelle, M., Leyser, O., 1998. Changes in auxin response
475 from mutations in an AUX/IAA gene. Science 279, 1371-1373.
476 Salehin, M., Bagchi, R., Estelle, M., 2015. SCFTIR1/AFB-based auxin perception: mechanism
477 and role in plant growth and development. The Plant Cell Online, tpc. 114.133744.
478 Scanlon, M.J., 2003. The polar auxin transport inhibitor N-1-naphthylphthalamic acid
479 disrupts leaf initiation, KNOX protein regulation, and formation of leaf margins in maize.
480 Plant Physiology 133, 597-605.
481 Scanlon, M.J., Schneeberger, R.G., Freeling, M., 1996. The maize mutant narrow sheath fails
482 to establish leaf margin identity in a meristematic domain. Development 122, 1683-1691.
483 Schindelin, J., Arganda-Carreras, I., Frise, E., Kaynig, V., Longair, M., Pietzsch, T., Preibisch, S.,
484 Rueden, C., Saalfeld, S., Schmid, B., 2012. Fiji: an open-source platform for biological-image
485 analysis. Nature methods 9, 676.
486 Sharman, B.C., 1942. Developmental anatomy of the shoot of *Zea mays* L. Annals of Botany
487 6, 245-282.
488 Smith, L.G., Greene, B., Veit, B., Hake, S., 1992. A dominant mutation in the maize homeobox
489 gene, *Knotted-1*, causes its ectopic expression in leaf cells with altered fates. Development
490 116, 21-30.
491 Strable, J., Wallace, J.G., Unger-Wallace, E., Briggs, S., Bradbury, P.J., Buckler, E.S., Vollbrecht,
492 E., 2017. Maize YABBY genes drooping leaf1 and drooping leaf2 regulate plant architecture.
493 The Plant Cell 29, 1622-1641.

494 Tan, X., Calderon-Villalobos, L.I.A., Sharon, M., Zheng, C., Robinson, C.V., Estelle, M., Zheng,
495 N., 2007. Mechanism of auxin perception by the TIR1 ubiquitin ligase. Nature 446, 640.
496 Temnykh, S., DeClerck, G., Lukashova, A., Lipovich, L., Cartinhour, S., McCouch, S., 2001.
497 Computational and experimental analysis of microsatellites in rice (Oryza sativa L.):
498 frequency, length variation, transposon associations, and genetic marker potential. Genome
499 research 11, 1441-1452.
500 Tian, Q., Nagpal, P., Reed, J.W., 2003. Regulation of Arabidopsis SHY2/IAA3 protein
501 turnover. The Plant Journal 36, 643-651.
502 Tian, Q., Reed, J.W., 1999. Control of auxin-regulated root development by the Arabidopsis
503 thaliana SHY2/IAA3 gene. Development 126, 711-721.
504 Tsuda, K., Abraham-Juarez, M., Maeno, A., Dong, Z., Aromdee, D., Meeley, R., Shiroishi, T.,
505 Nonomura, K., Hake, S., 2017. KNOTTED1 cofactors, BLH12 and BLH14, regulate internode
506 patterning and vein anastomosis in maize. The Plant Cell 10.1105/tpc.16.00967.
507 von Behrens, I., Komatsu, M., Zhang, Y., Berendzen, K.W., Niu, X., Sakai, H., Taramino, G.,
508 Hochholdinger, F., 2011. Rootless with undetectable meristem 1 encodes a monocot-
509 specific AUX/IAA protein that controls embryonic seminal and post-embryonic lateral root
510 initiation in maize. The Plant Journal 66, 341-353.
511 Wang, H., Jones, B., Li, Z., Frasse, P., Delalande, C., Regad, F., Chaabouni, S., Latche, A., Pech,
512 J.-C., Bouzayen, M., 2005. The tomato Aux/IAA transcription factor IAA9 is involved in fruit
513 development and leaf morphogenesis. The Plant Cell 17, 2676-2692.
514 Woll, K., Borsuk, L.A., Stransky, H., Nettleton, D., Schnable, P.S., Hochholdinger, F., 2005.
515 Isolation, characterization, and pericycle-specific transcriptome analyses of the novel
516 maize lateral and seminal root initiation mutant rum1. Plant Physiology 139, 1255-1267.
517 Worley, C.K., Zenser, N., Ramos, J., Rouse, D., Leyser, O., Theologis, A., Callis, J., 2000.
518 Degradation of Aux/IAA proteins is essential for normal auxin signalling. The Plant Journal
519 21, 553-562.
520 Yang, X., Lee, S., So, J.h., Dharmasiri, S., Dharmasiri, N., Ge, L., Jensen, C., Hangarter, R.,
521 Hobbie, L., Estelle, M., 2004. The IAA1 protein is encoded by AXR5 and is a substrate of
522 SCFTIR1. The Plant Journal 40, 772-782.
523 Zenser, N., Ellsmore, A., Leasure, C., Callis, J., 2001. Auxin modulates the degradation rate of
524 Aux/IAA proteins. Proceedings of the National Academy of Sciences 98, 11795-11800.

525 Zhang, Y., Marcon, C., Tai, H., von Behrens, I., Ludwig, Y., Hey, S., Berendzen, K.W.,
526 Hochholdinger, F., 2015. Conserved and unique features of the homeologous maize
527 Aux/IAA proteins ROOTLESS WITH UNDETECTABLE MERISTEM 1 and RUM1-like 1.
528 Journal of experimental botany 67, 1137-1147.
529
530
531 **Methods**
532 **Plant Growth Conditions**
533 Analyses were carried out in families segregating for *Hoja loca1* after at least four backcrosses to
534 the B73 inbred line. Plants were grown in Supersoil Brand Potting Soil (composted bark (60-85%),
535 Sawdust (60-85%), Sphagnum Peat Moss (10-30%)) in standard greenhouse conditions.
536 Seedlings were grown for 3 weeks in 30 by 45 by 2.5cm trays, and adult plants were grown in
537 12.5L pots until tassel emergence.
538
539 **Root Analysis**
540 Seeds were rehydrated overnight in sterile water, then sterilized with 10% bleach for 20 minutes,
541 before washing with sterile water. Seeds were then germinated on damp chromotography paper
542 in vertically fixed plastic wallets. After one week, the seedlings were photographed, then rotated
543 90°. The seedlings were left to grow for 24 hours and imaged every hour, for 12 hours. After 24
544 hours, the final root phenotype was imaged. Primary root length was analysed using FIJI
545 (Schindelin et al., 2012) and crown root number was counted. The seedlings were transplanted
546 to soil and three weeks after germination the shoot phenotype was recorded.
547
548 **Histology Plastic Sections**
549 10μm plastic sections were made with Technovit® 9100 from Electron Microscopy Services (Cat.
550 #14655) according to manufacturer instructions. Sections were mounted on glass slides and
551 stained with toluidine blue. Imaging was performed on a Zeiss Axiovert inverted compound
552 microscope with transmitted light.
553
554 **Scanning Electron Microscopy**
555 SEMs were performed with material fixed in FAA (3.7% formaldehyde, 50% ethanol, 5% acetic
556 acid) overnight at 4°C and dehydrated in ethanol series to 100%. Samples were critical point

557 dried, sputter coated with palladium, and imaged on a Hitachi S-4700 with 2kV accelerating
558 voltage.
559
560 **Tissue for Immunolocalisation and *In Situ* Hybridisation**
561 Plant tissue was collected from 3-week-old seedling shoot apices, dissected and fixed overnight
562 in 4% paraformaldehyde/ 0.1% DMSO/ 0.1% Triton-X100. Fixed samples were transferred
563 through an ethanol and histoclear series before embedding in paraplast plus (McCormick
564 Scientific #19216). 10μm sections of fixed tissue were mounted on probe-on-probe-plus slides
565 (FisherBrand #22-230-900) and dried overnight on a 37°C hotplate before use in either
566 immunolocalisation or *in situ* hybridization.
567
568 **Immunolocalisation**
569 Primary antibodies were guinea-pig anti-SoPIN1 as used in (Richardson et al., 2016) and rabbit
570 anti-KNOTTED1 (KN1) as used in (Bolduc et al., 2012b). Secondary antibodies were commercial
571 anti-guinea pig conjugated to Alexa-fluor594 (Jackson ImmunoResearch, #706-585-148) and
572 anti-rabbit alkaline phosphatase conjugate (Jackson ImmunoResearch, #111-055-045). All
573 antibodies were used at a 1:200 dilution in 1% bovine serum albumin (BSA) in PBS.
574 Immunolocalisation used a protocol based on (Conti and Bradley, 2007), and was as
575 follows. Slides were de-paraffinised using histoclear, then rehydrated through an ethanol series
576 to water. Samples were then boiled in 10mM sodium citrate, pH6, for 10 minutes to retrieve the
577 antigens. Blocking was carried out in 1% BSA/PBS/0.3% Triton-X100 for 3hours. Slides were
578 incubated overnight in primary antibody, before washing in PBS/0.3% Triton-X100. They were
579 then incubated with secondary antibody at room-temperature for 2 hours.
580 Tissues incubated with anti-KN1 were incubated in a 1:50 dilution of NBT/BCIP (Roche,
581 #11681451001) in 0.05M $MgCl_2$/TBS, pH9.5 until a dark precipitate was observed. These slides
582 were then imaged on a Leica dissecting microscope in water.
583 Tissues incubated with anti-SoPIN1 were stained for 20 minutes in 0.1% calcofluor
584 (fluorescent brightener 28, Sigma-Aldrich #F3543), washed and mounted in water and imaged on
585 a Leica SP8 confocal microscope. The subcellular localization of SoPIN1 was assessed in relation
586 to the calcofluor cell wall stain using FIJI (Schindelin et al., 2012).
587
588 ***In situ* Hybridisation**
589 Antisense probes targeted to *DROOPLING LEAF1* (GRMZM2G168893) mRNA were designed
590 as used in (Strable et al., 2017). *In situ* hybridization was carried out as in (Coen et al., 1990)

591 outlined here in brief. Tissue was deparaffinised using histoclear, then rehydrated through an
592 ethanol series. Samples were digested using 0.125mg/mL pronase (Sigma-Aldrich #P6611) in
593 50mMTris/5mM EDTA, pH7.5, for 15minutes at room temperature. Digestion was stopped by the
594 addition of 0.2% glycine before washing and re-fixing in 4% PFA/PBS for 10minutes. Slides were
595 then treated in 0.1M Triethanolamine-HCl / 0.5% Acetic Anhydride (Sigma-Aldrich #320102) for
596 10 minutes before dehydrating through an ethanol series. Tissue was incubated overnight with
597 the probes at a 1:50 dilution in hybridisation buffer (0.375M NaCl, 12.5mM Tris-HCl pH8, 12.5mM
598 Sodium Phosphate pH6.8, 6.25mM EDTA, 50% deionized formamide, 12.5% dextran sulfate,
599 1.25x Denhardt solution, 0.0125mg/mL tRNA) at 50°C. Slides were washed in 0.2% SSC at 50°C,
600 then treated with RNAseA (in 0.5M NaCl/10mM Tris/ 1mM EDTA, pH7.5) at 37°C for 15 mins,
601 before repeating the SSC washes. Slides were blocked in Roche Blocking Reagent (#11-096-
602 176-001) for 30 minutes, washed in1% BSA/0.3 % Triton-X100/TBS, and incubated at room-
603 temperature with a 1:500 dilution of anti-Dioxigenin-AP Fab fragments (Roche, #11093274910)
604 in 1% BSA/0.3 % Triton-X100/TBS for 1hour. Slides were then washed with in 1% BSA/0.3 %
605 Triton-X100/TBS, then in 0.05M $MgCl_2$/TBS, pH9.5. To visualize the probe localisation, the tissue
606 was incubated in 1:50 dilution of NBT/BCIP in 0.05M $MgCl_2$/TBS, pH9.5, until dark precipitate
607 formed. The staining reaction was stopped by transferring to water and the slides were imaged
608 on a Leica MZ16F microscope with a Qimaging Micropublisher camera under water and brightfield
609 conditions.
610
611 **Mapping with SSRs**
612 The *Oja* mutation was mapped to chromosome 3 using short sequence repeat (SSR) PCR
613 mapping. Known SSRs were identified using Maize gdb and are listed in Figure 3. Custom SSRs
614 were identified by using the Gramene SSR prediction tool (Temnykh et al., 2001), and specific
615 primers were designed to amplify them.
616
617 **Whole Genome Sequencing**
618 10 mm^2 area leaf discs were collected from 30 wild type and 30 mutant siblings in an advanced
619 B73 introgressed population. Genomic DNA was extracted using a UREA based extraction
620 method (Chen and Dellaporta, 1994) which is as follows. Tissue was ground in UREA extraction
621 buffer (4M urea, 4M NaCl, 1M Tris pH8, 0.5M EDTA, 34mM n-lauroyl sarcosine). Then an equal
622 volume of phenol:chloroform:isoamyl alcohol (25:24:1), was added and vortexed to mix. After
623 centrifugation, the supernatant was decanted and mixed with an equal volume of chloroform. After
624 centrifugation, the supernatant was decanted and mixed with $1/10^{th}$ volume of 4.4 M NH_4OAc pH

625 5.2 and 0.7 volume of isopropanol. Strands of DNA were then collected and washed with 70%
626 ethanol in a separate tube. The dried pellet was resuspended in 100ul of TE.
627 DNA was quantified using Qubit dsDNA HS Assay Kit (Invitrogen, Q32854), and sent to
628 Novogene for library preparation and sequencing (350bp insert, 150PE). Sequencing was at 10
629 times coverage of the maize genome. Sequence analysis was carried out using the CYVERSE
630 Atmosphere computing environment. The sequence data was quality checked and the adapters
631 trimmed using fastp, then aligned to the B73_RefGen_v3 maize genome using bowtie2, variants
632 were called using samtools mileup. The variant list was filtered using R, by removing variants
633 recorded in the Panzea HapMapv3 (https://hapmap.ncbi.nlm.nih.gov/) and those present in the
634 wild type pool as well as restricting to EMS type SNPs. Moderate and high effect SNPs specific
635 to the mutant were calculated using SNPEff2 with the B73v3 5b+ gene models.
636
637 **Vein Analysis**
638 Cross-sections through the third leaf of 3-week-old seedlings, 1.5cm above the ligule were taken
639 and imaged under water on a Leica DM4000 microscope. Cross-section images were analysed
640 using FIJI (Schindelin et al., 2012). The width of the leaf was recorded, then the number of lateral
641 and intermediate veins were counted. Vein density was calculated as the total number of veins
642 (lateral + intermediate veins) over the width of the leaf.
643 Vein distribution was assessed by counting the number of intermediate veins between
644 lateral veins. To align the wild type and midribless leaves, the lateral vein closest to the midpoint
645 of the leaf was designated at position 0, the “midvein”. Each lateral vein was then allocated a
646 position number in reference to position 0.
647
648 **Figures**

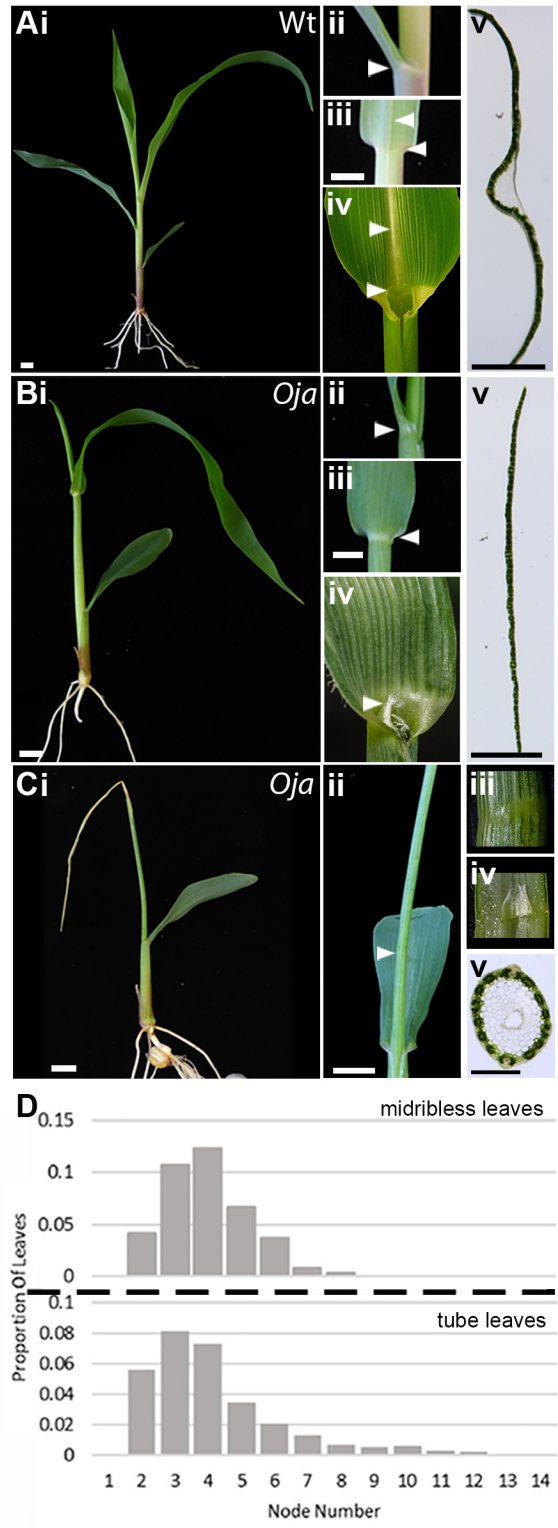

Figure 1. *Hoja loca1* mutants have leaf defects.

The phenotype of wild type (Wt) (A), mild (B) and severe (C) *Oja* mutants including (i) whole-seedling, and (ii-iv) magnified images of the ligule/ auricle regions, showing the side (ii) and abaxial (iii) and the adaxial (iv) views. (C iv) is a cross-section through the tube leaf showing the intact ligule (arrowhead). (v) Cross-sections through seedling leaves 1cm above the ligule. Scale bars are 1cm, arrowheads indicate the ligule or midrib regions. (D) The distribution of midribless and tube leaves in *Oja* plants (n=150), node 1 is at the base of the plant.

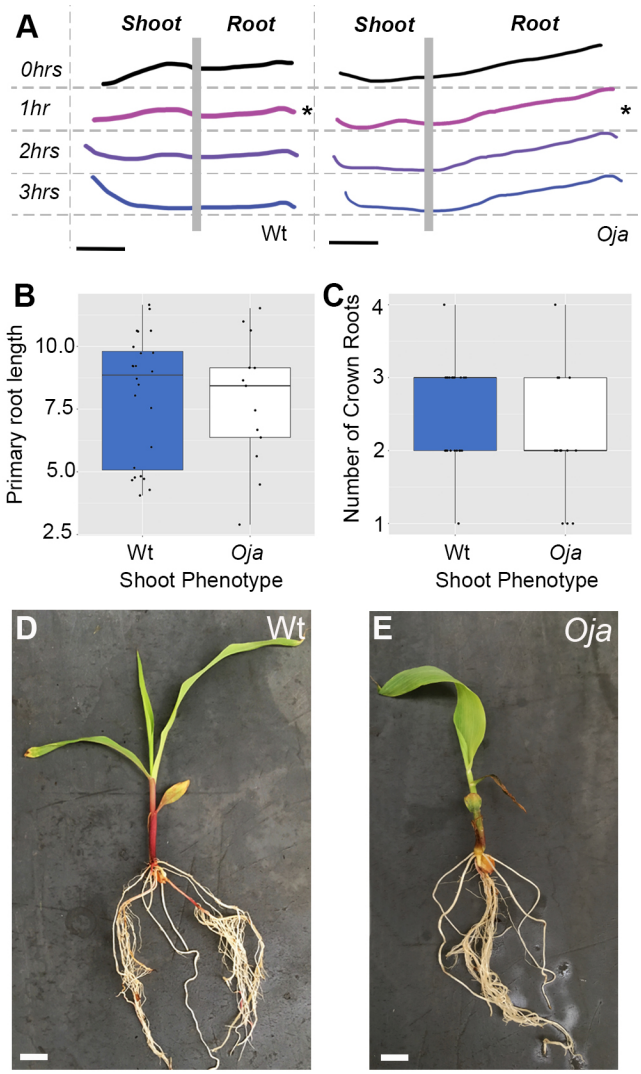

Figure 2. *Hoja loca1* mutants have a normal root phenotype.

(A) Oja seedling roots have a normal gravitropic response, showing a change in root tip orientation by 1 hour after turning (*) (scale bars are 2cm). (B-C) Root architecture in 1.5-week-old seedlings is not significantly different between wild-type and *Oja* plants, as shown by primary root length (B, Welch 2-sample t-test, df=24, n *Oja*=13, Wt=24, p=0.853) and number of initiating crown roots (C, Welch 2-sample t-test, df=19, n *Oja*=13, Wt=24, p=0.1452). (D-E) Root architecture in 3-week-old seedlings appears to be similar between mutant and normal sibling (Wt) (scale bars are 2cm).

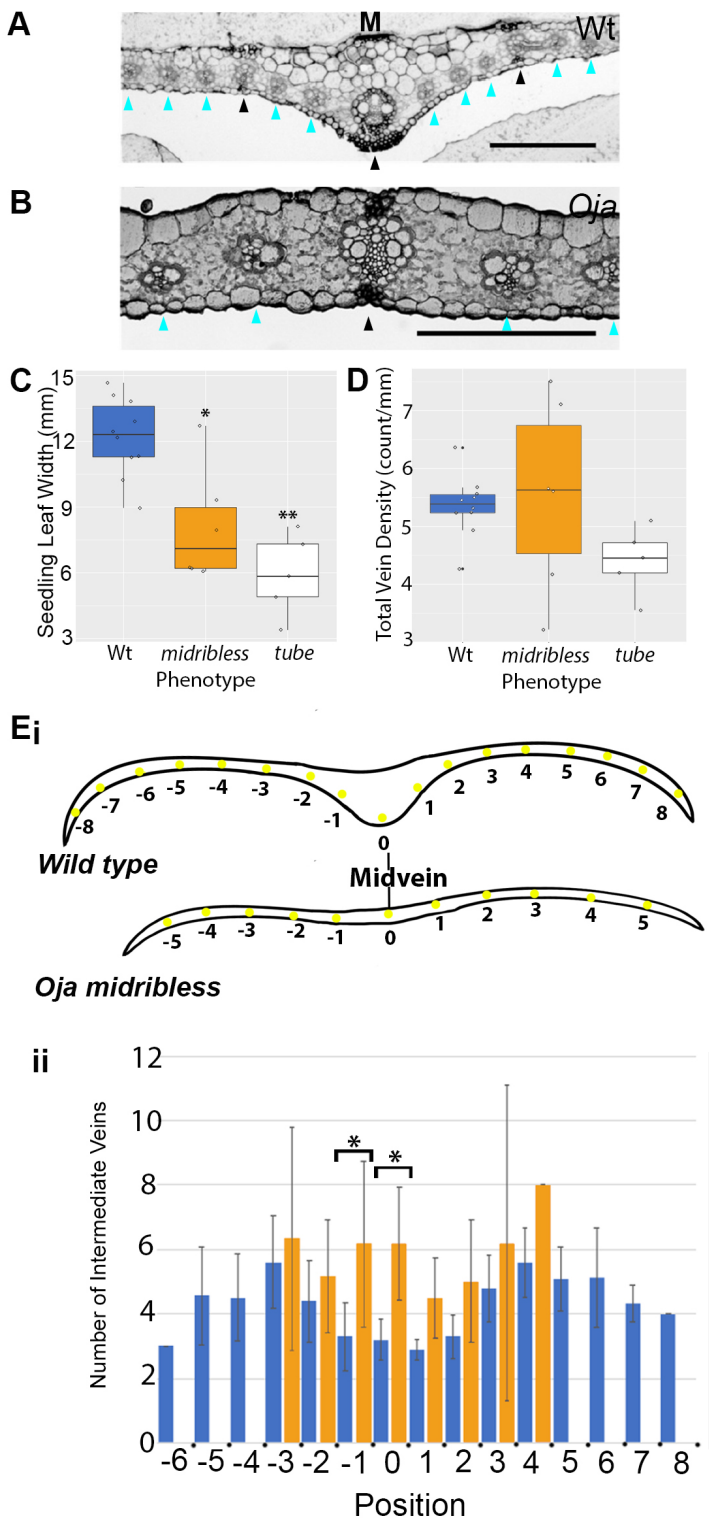

Figure 3. *Hoja loca1* mutants have a defect in vein distribution.

(A-B) Plastic sections through wild type (A) and midribless (B) leaves. The midrib is indicated by the M, the lateral veins by the black arrowheads, and intermediate veins by the cyan arrowheads. Scale bars are 1mm. (C) Seedling leaf width varies significantly between wild type and midribless (n=10 of each phenotype, ANOVA and Tukeys HSD, df=2, * p= 0.0032) and between wild type and tube leaves (**, p=0.000083). (D) Total leaf vein density does not vary significantly. (E) Leaf vein distribution is perturbed in midribless mutants. (Ei) Cartoons depicting the alignment of midribless and wild-type leaves. Wild type and mutant leaves were aligned by allocating the position of “0” to the wild type midvein, and the lateral vein closest to the midpoint of the leaf in the midribless mutant. Each successive lateral vein was then allocated a position relative to 0 (Ei) and the number of intermediate veins between each position was recorded. (Eii) The mean number of intermediate veins near the midvein

726 were significantly different in the midribless mutant (orange) when compared to wild type (blue)
727 (n=10 for each phenotype, ANOVA and Tukeys HSD, * p = 0.0051 and p=0.00089).
728

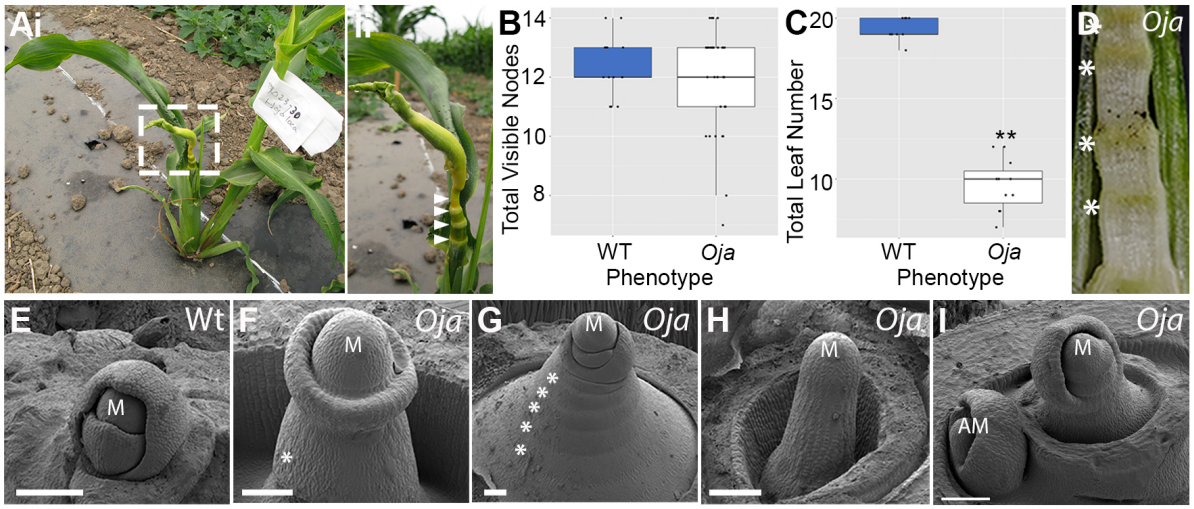

729

730 **Figure 4. *Hoja loca1* mutants initiate new phytomers but fail to initiate leaves.**
731 (A-C) Mature *Oja* plants are often short, and despite having a similar number of visible nodes (B,
732 p=0.2537, Welch's 2-Sample T-Test, df= 39.8, n *Oja*=29, Wt=14), they have fewer leaves (C, **
733 p= 4.17e-11, Welch's 2-Sample T-Test, df=14.194, n= 10 of each phenotype) than wild type. In
734 particular, the nodes below the tassel are often bare (Aii, arrowheads). Bare nodes can also be
735 identified in cross-sections through developing shoots (D). The lack of leaf initiation is clear at the
736 earliest stages of development. Scanning electron micrographs (SEMs) of wild type (E) and
737 mutant (F-I) vegetative meristems with attached leaf primordia show severe defects in *Oja*. Some
738 leaf primordia fail to arch over the meristem, instead forming a ring-shaped primordium (F). Some
739 have clear ridges where internodes have formed below the meristem (G), which would normally
740 be concealed by leaves in wild-type plants. Other mutants form pin-shaped meristems (H). Often
741 the tiller buds in *Oja* are normal (I) allowing the plant to produce progeny. The internodes are
742 indicated by the *, meristems by 'M', axillary meristems by 'AM'. Scale bars are 100μm.
743

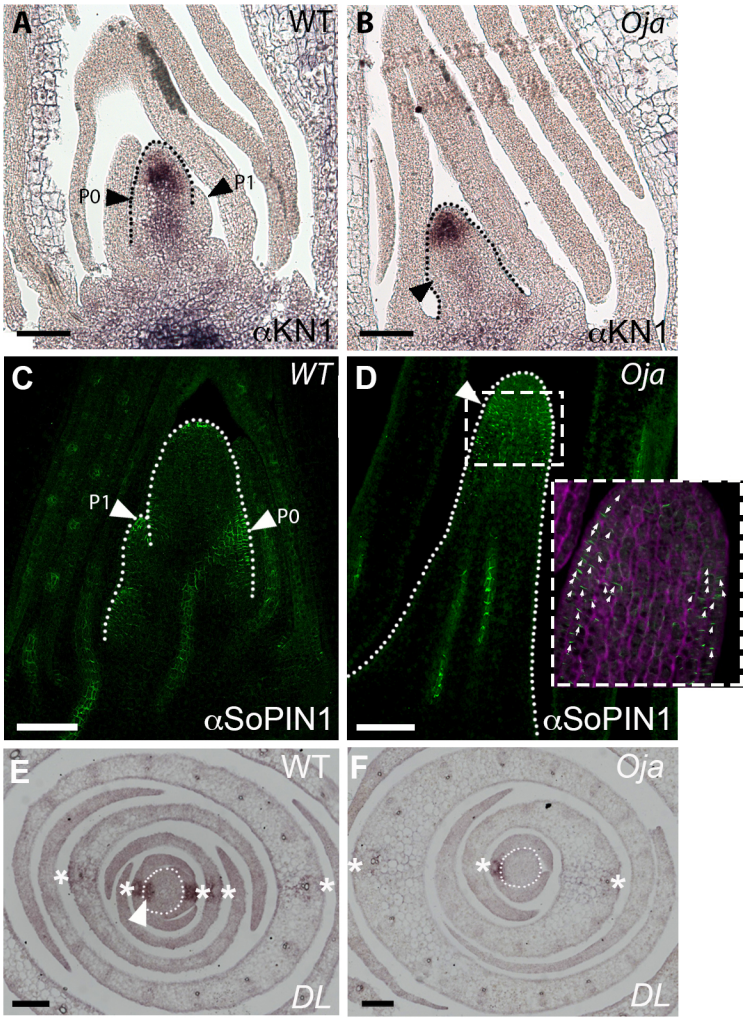

Figure 5. *Hoja loca1* have defects in organ initiation markers localization. KNOTTED1 (KN1) immunolocalisation (dark brown/black, A-B) and SISTER OF PINFORMED1 (SoPIN1, green, C-D) in longitudinal sections through 3-week-old seedlings in WT (A,C) and mutant (B,D) plants. The inset in D shows a magnified image of the boxed region, the arrowheads indicate the orientation of the SoPIN1 localization (green) within the cell outline (magenta). Large arrowheads indicate the P_0 and P_1 domains. Dotted lines indicate the outline of the meristem region. The white dotted line in A indicate the P_0. (E-F) *In situ* hybridization of *drooping leaf* (dark brown, DL) in transverse cross-sections through 3-week-old seedlings, in wild type (E) and mutant (F) plants. Sections are 100μm from the tip of the meristem. * indicate the position of the midvein in successive leaves, the white dotted line outlines the meristem. Scale bars are 100μm.

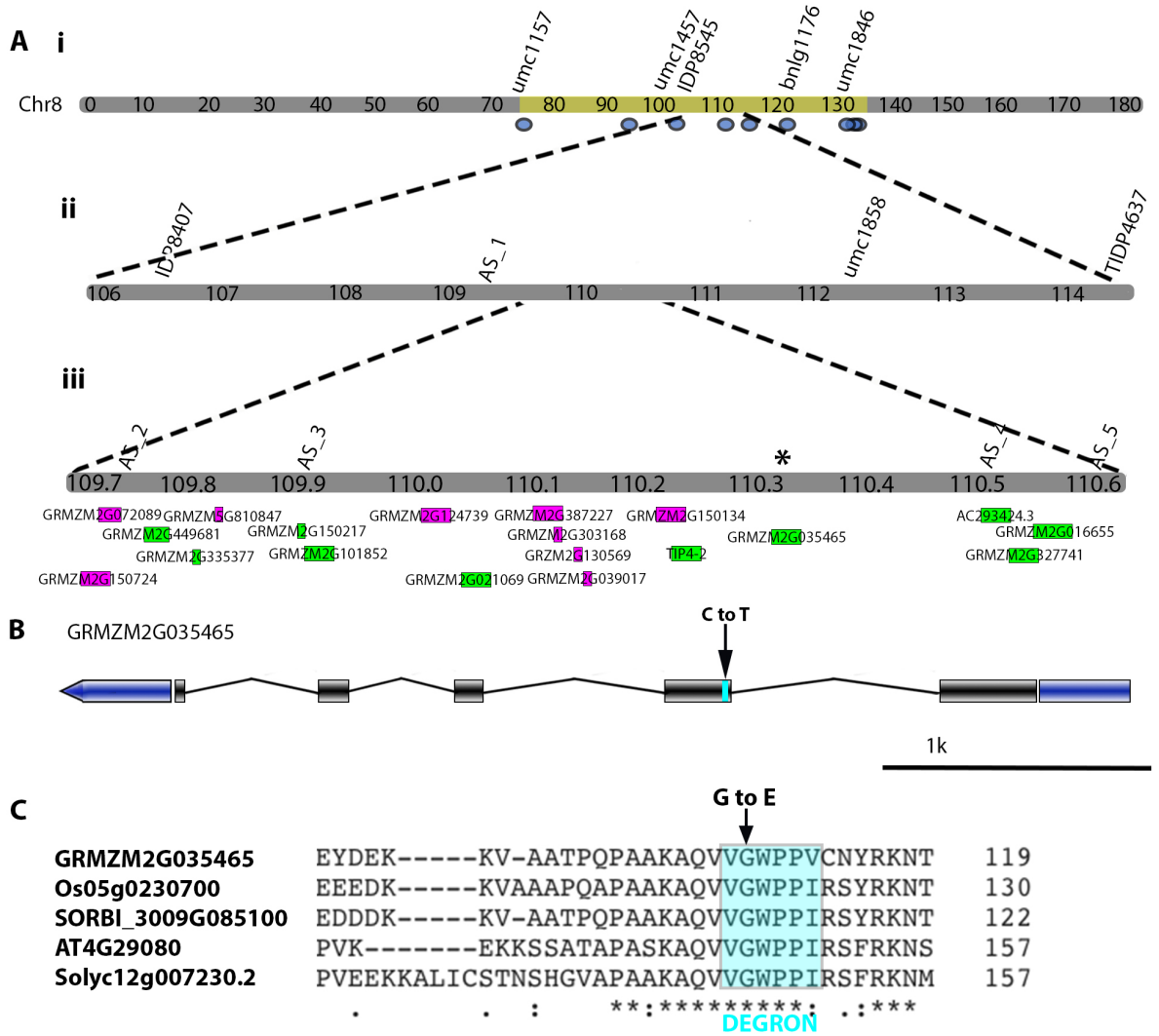

Figure 6. *Hoja loca1* maps to ZmIAA28 on Chr8.

Using short sequence repeat (SSR) PCR markers, *Oja* was mapped to Chr8 between 109.7-110.6Mb (A). Custom SSR markers are labeled as 'AS#'. Of the 19 genes in the fine mapping interval (Aiii), 10 are expressed in shoot meristems and leaf primordia (green), 9 are not (magenta) based on published RNAseq datasets. Whole genome sequencing (WGS) data identified 9 high to moderate effect SNPs in gene bodies in the larger mapping region (Ai, blue ovals, Chr8:75-135Mb). Of these, only one is an EMS-type SNP that falls within the fine mapping interval (Aiii, *). The SNP causes a C to T change in the second exon of GRMZM2G035465, ZmIAA28 which results in a glycine to glutamic acid amino acid change in the highly conserved degron motif (C, cyan box).

Supplementary Figures

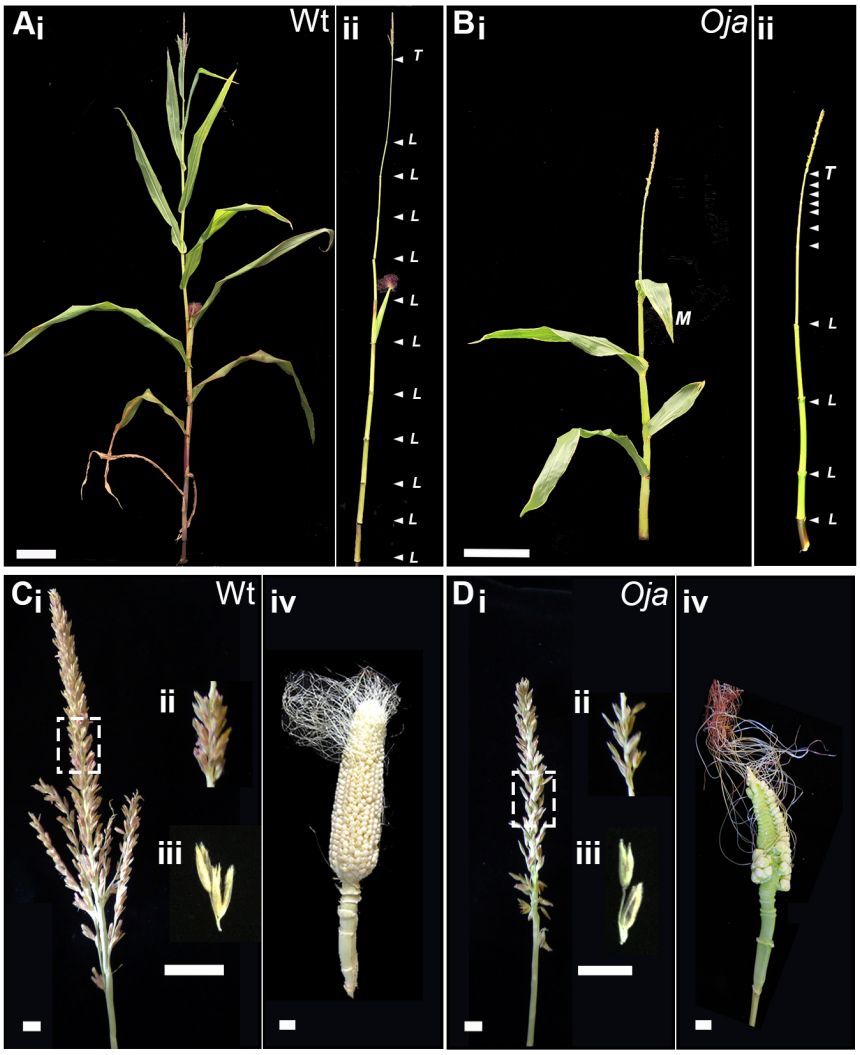

Supplementary Figure 1. *Hoja loca1* Mature Phenotype.

The mature phenotype of a wild type (A) and mutant (B) plant, with leaves attached (i) and removed (ii), scale bar is 15cm. The positions of nodes are indicated by the white arrowheads, those that have a leaf are indicated by “L” and the base of the tassel is indicated by “T”. The phenotype of tassels and ears in wild type (C) and mutant (D) plants. (i) Whole tassel, (ii) zoomed-in image of the boxed region, (iii) an individual spikelet pair, (iv) unfertilized ear. Scale bars are 1cm.